Int. J. Bio-Inorg. Hybd. Nanomat., Vol. 1, No. 4 (2012), 215-226

International Journal of Bio-Inorganic Hybrid Nanomaterials

Lu^{3+}/Yb^{3+} and Lu^{3+}/Er^{3+} Co-doped Antimony Selenide Nanomaterials: Synthesis, Characterization, Electrical, Thermoelectrical and Optical Properties

Sang Woo Joo[1*], Younes Hanifehpour[1], Bong-Ki Min[2]

[1] School of Mechanical Engineering, WCU Nano Research Center, Yeungnam University, Gyongsan 712-749 South Korea

[2] Center for Research Facilities, Yeungnam University, Gyeongsan712-749, South Korea

Received: 18 September 2012; Accepted: 22 November 2012

ABSTRACT

Lu^{3+}/Yb^{3+} and Lu^{3+}/Er^{3+} Co-doped Sb_2Se_3 nanomaterials were synthesized by a Co-reduction method in hydrothermal condition. Powder XRD patterns indicate that the $Ln_xLn'_xSb_{2-2x}Se_3$ Ln: Lu^{3+}/Yb^{3+} and Lu^{3+}/Er^{3+} crystals (x= 0.00-0.04) are isostructural with Sb_2Se_3. The cell parameters were increased for compounds upon increasing the dopant content (x). SEM and TEM images show that Co-doping of Lu^{3+}/Yb^{3+} ions in the lattice of Sb_2Se_3 results in nanorods while that in Lu^{3+}/Er^{3+} leads to nanoparticles, respectively. The electrical conductivity of Co-doped Sb_2Se_3 is higher than the pure Sb_2Se_3, and increases with temperature. By increasing concentration of Ln^{3+} ions, the absorption spectrum of Sb_2Se_3 shows red shifts and someintensity changes. In addition to the characteristic red emission peaks of Sb_2Se_3, emission spectra of Co-doped materials show other emission bands originating from f-f transitions of the Yb^{3+} ions.

Keyword: Co-doped; Nanomaterial; Luminescent; Electrical conductivity; Semiconductor.

1. INTRODUCTION

Nanosized semiconductor materials have drawn much research attention because their physical and chemical properties, due to size quantization effect, dramatically change and, in most case, are improved as compared with their bulk counterparts [1-3]. Rare earth substituted compounds with various compositions have become an increasingly important research topic in diverse areas, such as luminescent device, light emitting displays, biological labeling and imaging [4-6] due to the introduction of dopant levels within the band gap and modification of the band structure. In addition,

(*) Corresponding Author - e-mail: swjoo@yu.ac.kr

significant efforts have been devoted to enhance the activity of wide band gap photocatalysts by doping for environmental remediation [7, 8]. emiconductor selenides find applications as laser materials, optical filters, sensors, and solar cells. Antimony selenide, an important member of these V_2VI_3 compounds, is a layer structured semi-conductor of orthorhombic crystal structure, and exhibits good photovoltaic properties and high thermoelectric power (TEP), which allows possible applications for optical and thermoelectronic cooling devices [9-11]. The research of impurity effects or doping agents on the physical properties of Sb_2Se_3 is interesting both for basic and applied research. Doping of some transition metal and lanthanide to the lattice of metal chalcogenides has been investigated [12-17]. The incorporation of large electropositive ions such as lanthanides into metal chalcogenide frameworks is expected to affect the electronic properties of that framework. In this work, we report preparation, structural, electrical and optical properties of Lu^{3+}/Yb^{3+} and Lu^{3+}/Er^{3+} Co-doped antimony selenide via co-reduction method at hydrothermal condition.

2. EXPERIMENTAL

All chemicals were of analytical grade, and were used without further purification. Grey selenium (1 mmol) and NaOH (5 mmol) were added to distilled water (60 mL), and stirred well for 10 min at room temperature. Afterwards, hydrazinium hydroxide (2 mL, 40 mmol), $SbCl_3$ (1.98, 1.96, 1.94, 1.92 mmol) and Ln_2O_3 (0.00, 0.01, 0.02, 0.04 mmol) (Ln: Lu^{3+}, Yb^{3+}, Er^{3+}) based on molecular formula $Ln_xLn'_xSb_{2-2x}Se_3$ (x= 0.04) were added, and the mixture was transferred to a 100 mL Teflon-lined autoclave. The autoclave was sealed, maintained at 180°C for 48 h, and then cooled to room temperature. The optimum conditions for this reaction are pH= 12, temperature 180°C and reaction time 48 h. The black precipitate obtained was filtered and washed with ethanol and water. It was dried at room temperature. Yields for the products were 75-85%. Phase identification was performed with an X-ray powder diffractometer (XRD D5000 Siemens) with Cu-K_α radiation. Cell parameters were calculated with Celref program from powder XRD patterns, and reflections have been determined and fitted using a profile fitting procedure with the Winxpow program. The reflections observed in 2θ= 4-70° were used for the lattice parameter determination. The morphology of materials was examined by a scanning electron microscope SEM (Hitachi S-4200). A linked ISIS-300, Oxford EDS (energy dispersion spectroscopy) detector was used for elemental analyses .The HRTEM image and SAED pattern were recorded by a Cs-corrected high-resolution TEM (JEM-2200FS, JEOL) operated at 200 kV. Photoluminescence measurements were carried out using a SpexFluoroMax-3 spectrometer after dispersing a trace amount of sample via ultrasound in distilled water. The Four Probe Method was used for the measurement of electrical and thermoelectrical resistivity of samples. A small oven was needed for the variation of temperature of the samples from the room temperature to about 200°C (max.). Small chip with 1mm thickness and 7 mm length was used for this analysis.

3. RESULTS AND DISCUSSION

The powder X-ray diffraction (P-XRD) patterns (Figure 1) of $Lu_xYb_xSb_{2-2x}Se_3$ samples indicate that the Lu^{3+}/Yb^{3+} Co-doped antimony selenide have the same orthorhombic structure as Sb_2Se_3 and that single phase Sb_2Se_3 is retained at lower doping concentrations of Lu^{3+}/Yb^{3+}. All the peaks in the Figure 1 can be attributed to the orthorhombic phase of Sb_2Se_3 with pbnm space group and lattice parameters a= 11.62Å, b= 11.76 Å and c= 3.95Å (JCPDS card File:72-1184). For doping levels higher than x= 0.04 for Lu^{3+} and Yb^{3+} additional unknown phases were observed (Figure 1c). In case of Lu^{3+}/Er^{3+} Co-doped compounds the intensity of some peaks has been changed and for doping levels higher than of x= 0.04 for Lu^{3+} and Er^{3+} additional unknown phases were also observed (supplementary data).

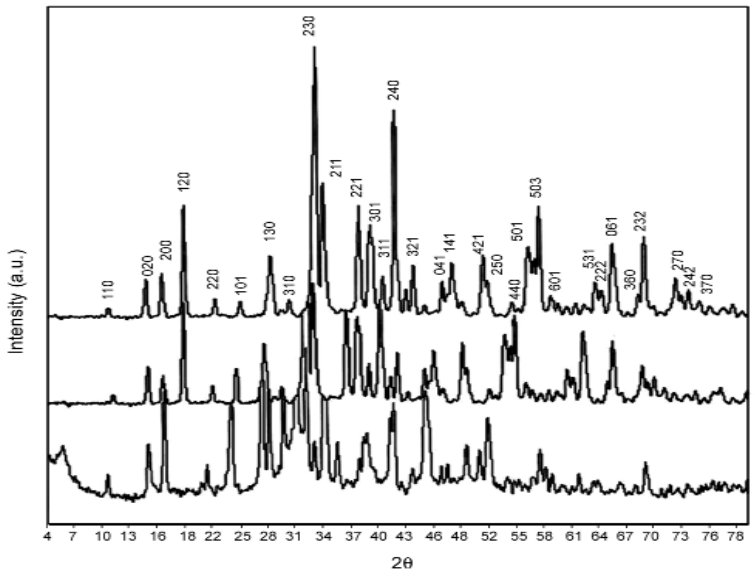

Figure 1: *Powder X-ray diffraction pattern of $Lu_xYb_xSb_{2-x}Se_3$ (a: x= 0.0, b: x= 0.04, c= unknown impurity phase) synthesized at 180°C and 48 h.*

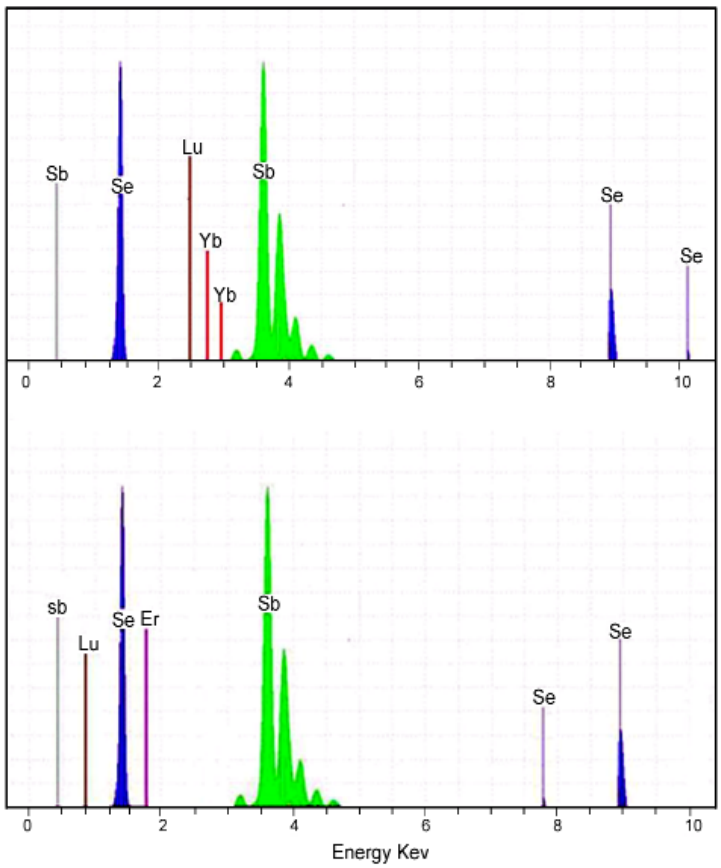

Figure 2: *EDX patterns of $Ln_xLn'_xSb_{2-2x}Se_3$ compounds.*

In addition, a little shift toward low angle was seen in the diffraction peaks of the Co-doped Sb_2Se_3 compared with those of undoped Sb_2Se_3 nano- crystals. This suggests that the larger lanthanide ions substitute the antimony ions, resulting in increased lattice constants. As expected, the EDX and ICP analysis of the product confirms the ratio of Sb/Se/Ln/Ln′ (see Figure 2).

The cell parameters of the synthesized materials were calculated from the XRD patterns. With increasing dopant content (x), the lattice parameters were increased for these materials, as shown in Figure 3.

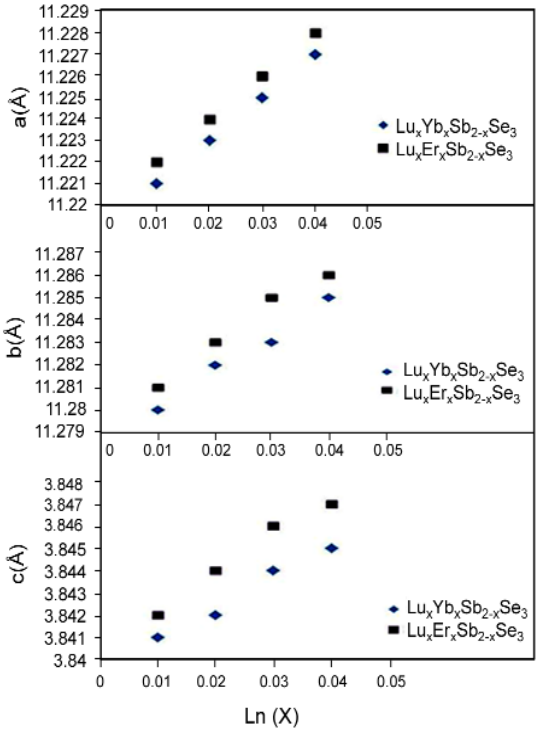

Figure 3: *The lattice constants of Co-doped Sb_2Se_3 dependent upon Ln^{3+}doping on Sb^{3+}sites.*

Figure 4 shows SEM images of $Lu_{0.04}Yb_{0.04}Sb_{1.92}Se_3$ nanorods with 3 μm lengths and thicknesses of 70-200 nm. Co-doping of Lu^{3+} and Yb^{3+} into the structure of Sb_2Se_3 does not change the morphology of Sb_2Se3 nanorods, but doping of Lu^{3+} and Er^{3+} into the structure of Sb_2Se_3 changes the morphology from rods to particles. The diameter of $Lu_{0.04}Er_{0.04}Sb_{1.92}Se_3$ particles is around 25 nm (Figure 5).

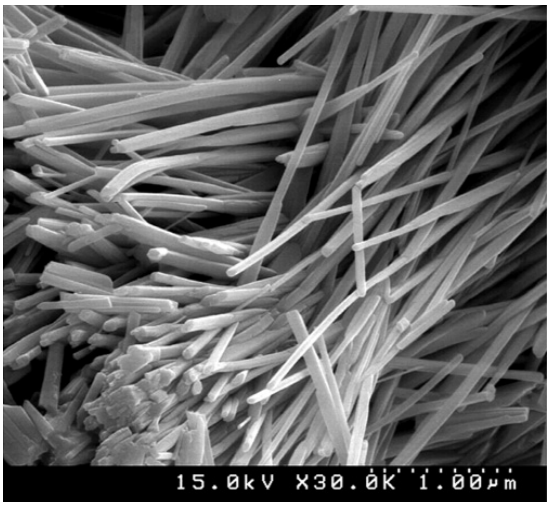

Figure 4: *SEM image of $Lu_{0.04}Yb_{0.04}Sb_{1.92}Se_3$ nanorods.*

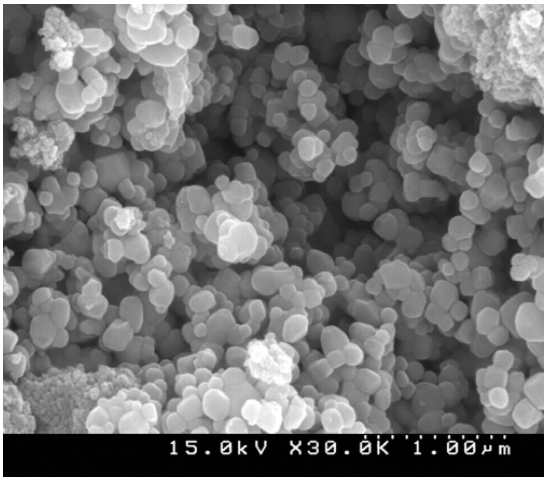

Figure 5: *SEM image of $Lu_{0.04}Er_{0.04}Sb_{1.92}Se_3$ nanoparticles.*

Figure 6a shows TEM image of as-prepared $Lu_{0.04}Yb_{0.0}4Sb_{1.92}Se_3$ nanorods. The Selected Area Electron Diffraction pattern (SAED) and typical HRTEM image recorded from the same nanorods of $Lu_{0.04}Yb_{0.04}Sb_{1.92}Se_3$ is shown in Figures 6b and 6c. The crystal lattice fringes are clearly observed and average distance between the neighboring fringes is 0.82 nm, corresponding to the [10-1] plane lattice distance of orthorhombic-structured Sb_2Se_3, which suggests that $Lu_{0.04}Yb_{0.04}Sb_{1.92}Se_3$ nanorods grow along the

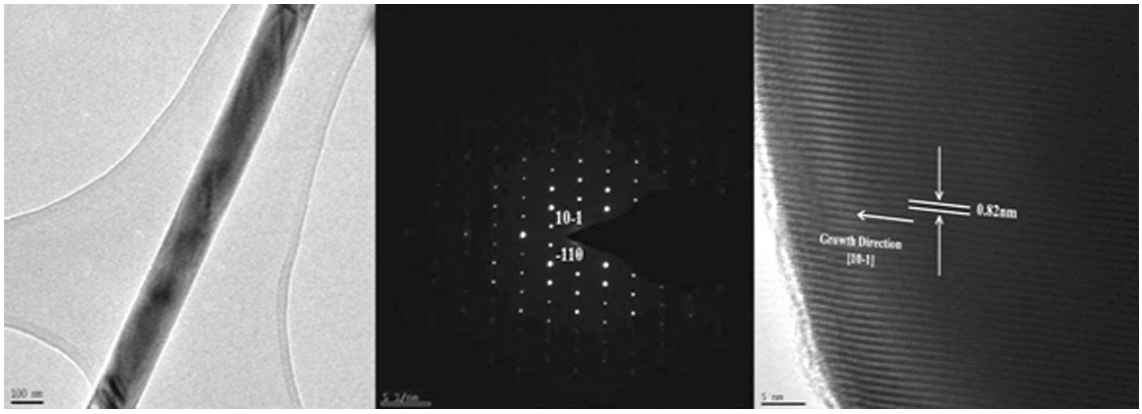

(a) (b) (c)

Figure 6: *The TEM (a), SAED pattern (b) and HRTEM image (c) of* $Lu_{0.04}Yb_{0.04}Sb_{1.92}Se_3$ *nanorods.*

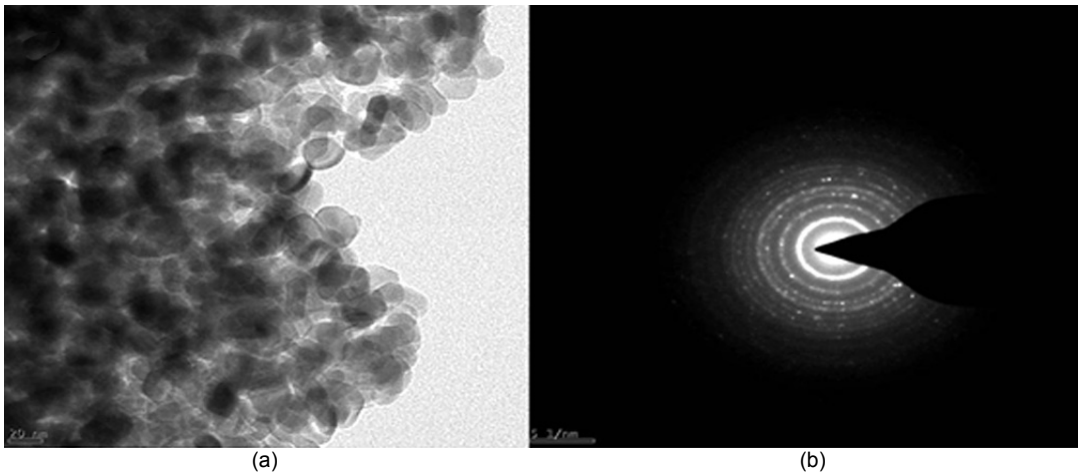

(a) (b)

Figure 7: *The TEM (a), and SAED pattern (b) of* $Lu_{0.04}Er_{0.04}Sb_{1.92}Se_3$ *nanoparticle.*

[10-1] direction. The HRTEM image and SAED pattern is the same for Sb_2Se_3 and show the similar growth direction (see the supplementary data).

Figures 7a and 7b show TEM image and SAED patterns of $Lu_{0.04}Er_{0.04}Sb_{1.92}Se_3$ nanoparticles obtained in ethanol/water media that confirms the result through SEM images and shows high crystallinity of sample.

In doped semiconductors, two types of emissions are responsible for the dopant (impurity) luminescence. One can be observed only upon direct excitation of the dopant. The other type is obtained if energy transfer from host to dopant occurs. Binary compounds such as Sb_2Se_3 and its alloys are thermoelectric materials with layered crystalline structures. These materials have been investigated for direct conversion of thermal energy to electric energy and they specially are used for electronic refrigeration [9].

The Four Probe Method was used for the measurement of electrical and thermoelectrical resistivity of samples (Scheme 1).

At room temperature the electrical resistivity of pure Sb_2Se_3 was of the order of 0.2 Ωm and in the case of $Lu_{0.04}Yb_{0.04}Sb_{1.92}Se_3$ the minimum value of electrical resistivity is 0.009 Ωm, and for

$Lu_{0.04}Yb_{0.04}Sb_{1.92}Se_3$ are 0.032 Ωm, respectively. With the increase in the lanthanide concentration, the electrical resistivity of synthesized nano-materials decreased obviously (Figure 8).

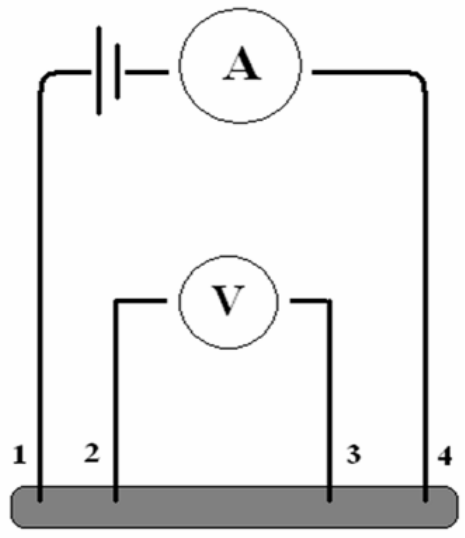

Scheme1: *Schematic of Four-Point Probe.*

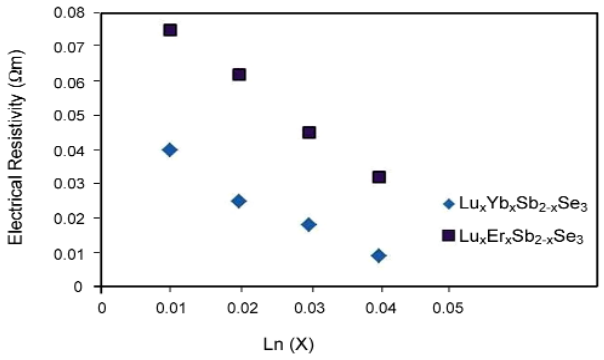

Figure 8: *Electrical resistivity of Co-doped Sb_2Se_3 compounds.*

The temperature dependence of the electrical resistivity for Co-doped Sb_2Se_3 nanomaterials between 290 and 350 K is shown in Figure 9. Electrical resistivity decreases linearly with temperature and the minimum value for $Lu_{0.04}Yb_{0.04}Sb_{1.92}Se_3$ was measured 0.0006 Ωm and for $Lu_{0.04}Er_{0.04}Sb_{1.92}Se_3$ 0.005 Ωm, respectively. Two factors including overlapping of wave functions of electrons in doped Sb_2Se_3 and acting as a charge carrier due to lanthanide atomic structure (having empty f orbitals) are important reasons for decreasing electrical resistivity. The obtained data shows higher electrical resistivity for Co-doped samples in comparison to doped samples in case of Lu^{3+}, Yb^{3+} and Er^{3+} doped Sb_2Se_3 [16, 17].

Comparing doped and Co-doped data, combining energy levels of two lanthanides and overlapping of wave functions of electrons in two different lanthanides are responsible for the difference between obtained results. Among Co-doped compounds, Lu^{3+}/Yb^{3+}-doped Sb_2Se_3 has the higher electrical conductivity.

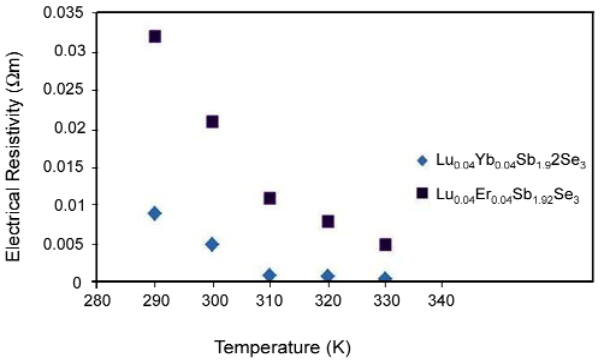

Figure 9: *Thermoelectrical resistivity of Co-doped Sb_2Se_3 compounds.*

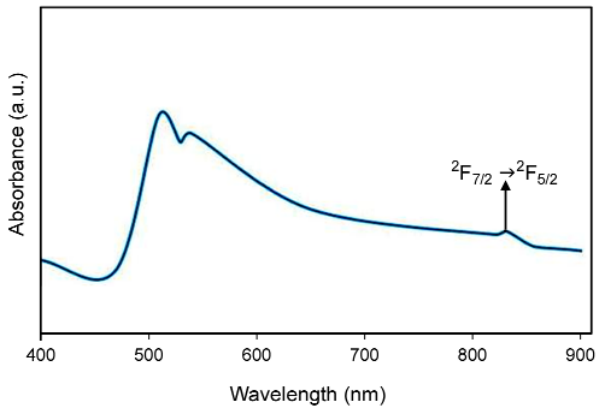

Figure 10: *Absorption spectra of $Lu_{0.04}Yb_{0.04}Sb_{1.92}$ Se_3 nanorods at room temperature.*

UV/Vis spectra of $Lu_{0.04}Yb_{0.04}Sb_{1.92}Se_3$ are shown in Figure 10. Absorption spectra reveal the

existence of Sb_2Se_3 and Lu^{3+} ions at (in the visible domain) and Yb^{3+} ions in the near-IR domain. By increasing concentration of Ln^{3+} ions, the absorption spectrum of Sb_2Se_3 shows red shifts and some intensity changes (see supplementary data). The Lu^{3+} ion has no excited 4f levels and therefore, the peaks between 500-600 nm can be assigned to ionization of Lu 5d orbitals and lattice of Sb_2Se_3 [18, 19] and the peak at 830nm can be assigned to the $^2F_{7/2}\rightarrow{}^2F_{5/2}$ transition (f-f transitions) of theYb^{3+} ions [20]. For $Lu_{0.04}Er_{0.04}Sb_{1.92}Se_3$, transition of the Er_{3+} ions is not observed because of instrument limitation. Then the peaks between 500-620 nm can be assigned to lattice of Sb_2Se_3 (Figure 11). The difference between absorption patterns of compound is related to various defects created in lattice. There is a red shift in doped materials in comparison to pure Sb_2Se_3 because of the smaller nanoparticles of Sb_2Se_3, in which band gap is higher than the doped nanomaterials [21, 22].

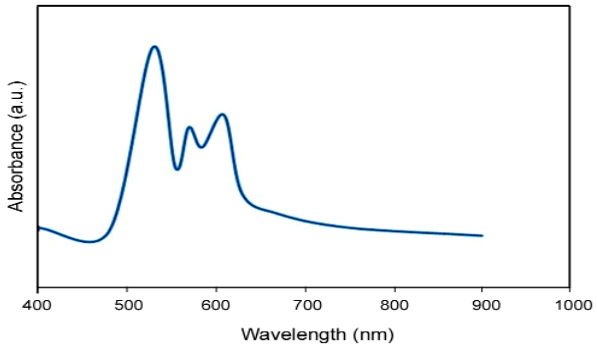

Figure 11: *Absorption spectra of $Lu_{0.04}Er_{0.04}Sb_{1.92}$ Se_3 nanoparticles at room temperature.*

It is well known that the fundamental absorption can be used to determine the nature and value of the optical band gap of the nanoparticles. The band gap energies of samples were estimated from the absorption limit. The calculated band gap is 2.43 eV for $Lu_{0.04}Yb_{0.04}Sb_{1.92}Se_3$ and 2.36 eV for $Lu_{0.04}Er_{0.04}Sb_{1.92}Se_3$. Figure 12 exhibited the RT PL emission spectra of $Lu_{0.04}Yb_{0.04}Sb_{1.92}Se_3$. The Lu^{3+} 5d-4f luminescence is almost completely quenched at temperatures T > 200 K. The Lu^{3+} ion has no excited 4f levels, and therefore thermal quenching of Lu^{3+} 5d-4f luminescence cannot be caused by nonradiative transitions to 4f levels, and should be attributed to thermally activated ionization of 5d electrons to the conduction band [18, 19]. Then, the peaks at 500-700 nm can be assigned to crystal structure of Sb_2Se_3 and its defects and the band 880 nm is related to $^2F_{5/2}\rightarrow{}^2F_{7/2}$ transition of Yb^{3+} ions. In case of $Lu_{0.04}Er_{0.04}Sb_{1.92}Se_3$ intra-4f Er^{3+} transitions of the $^4I_{11/2}$ and $^4I_{13/2}$ levels to the ground state ($^4I_{15/2}$) are expected around 1.54 μm. These could, however, not be determined due to equipment limitations [21]. Therefore emission bands at 550-700 nm is related to crystal structure of Sb_2Se_3 (Figure 13).

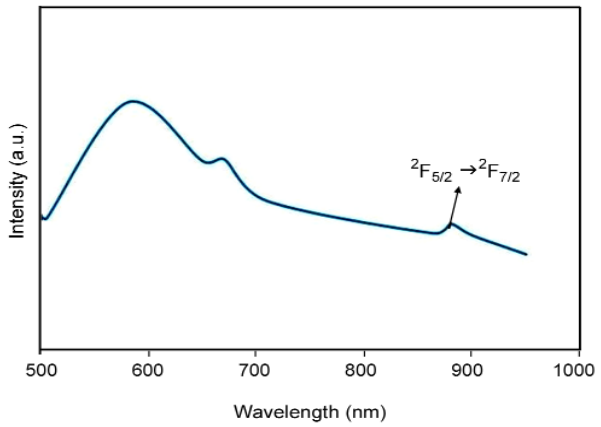

Figure 12: *Emission spectra for $Lu_{0.04}Yb_{0.04}Sb_{1.92}$ Se3 nanorods at room temperature (λ_{exc}= 470 nm).*

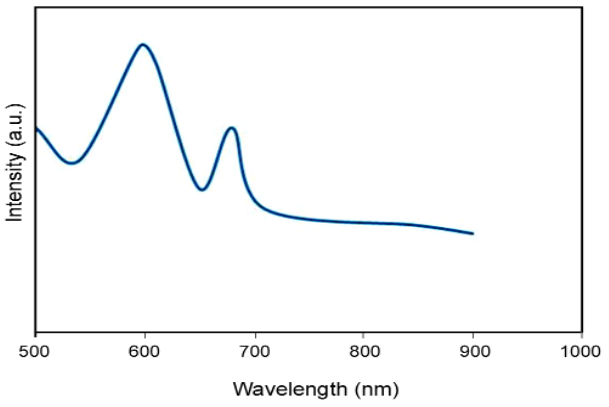

Figure 13: *Emission spectra for $Lu_{0.04}Er_{0.04}Sb_{1.92}Se_3$ nanoparticles at room temperature (λ_{exc}= 495 nm).*

4. CONCLUSIONS

New thermoelectric $Ln_{2x}Sb_{2-2x}Se_3$ (Ln: Lu^{3+}/Yb^{3+} and Lu^{3+}/Er^{3+}) based nanomaterials were synthesized by a simple hydrothermal method. The cell parameters were increased for compounds upon increasing the dopant content (x). According to SEM and TEM images, different morphologies were seen in Co-doped Sb_2Se_3. The HRTEM image and SAED pattern shows the similar growth direction along [10-1] for Lu^{3+}/Yb^{3+} Co-doped like Sb_2Se_3 nanorods. Lanthanide doping promotes the electrical conductivity of Sb_2Se_3 as well as thermoelectrical conductivity. UV-Vis absorption and emission spectroscopy reveals mainly electronic transitions of the Ln^{3+} ions in case of Yb^{3+} doped nanomaterials.

SUPPORTING INFORMATION

XRD patterns of $Lu_xEr_xSb_{2-2x}Se_3$, TEM, HRTEM images, SAED pattern of Sb_2Se_3 nanorods, absorption spectra of $Lu_{0.02}Yb_{0.02}Sb_{1.96}Se_3$, $Lu_{0.01}Yb_{0.01}Sb_{1.98}Se_3$ and $Lu_{0.02}$ $Er_{0.02}Sb_{1.96}Se_3$ are provided.

ACKNOWLEDGMENT

This work is supported by the Grant 2011-0014246 of the National Research Foundation of Korea.

REFERENCES

1. Calvert P., *Nature*, **383**(1996), 300.
2. Weller H., *Adv. Mater.*, **5**(1993), 88.
3. Alivisatos A.P., *Science*, **271**(1996), 933.
4. Wang F., Han Y., Lim C.S., Lu Y.H., Wang J., Xu J., Chen H.Y., *Nature*, **463**(2010), 1061.
5. Tachikawa T., Ishigaki T., Li J., Fujitsuka M., *Angew. Chem. Int. Ed.*, **47**(2008), 5348.
6. Sun Y., Chen Y., Tian L.J., Yu Y., Kong X.G., *J. Lumin.*, **128**(2008), 15.
7. Batzill M., Morales E.H., Diebold U., *Phys. Rev. Lett.*, **96**(2006), 026103.
8. Asahi R., Morikawa T., Ohwaki T., Aoki K., Taga Y., *Science*, **293**(2001), 269.
9. Chim T., Chun B., *J. Alloys Compd.*, **437**(2007), 225.
10. Qiu X., Burda C., Fu R., Zhu J., *J. Am. Chem. Soc*., **126**(2004), 16276.
11. Mastrovito C., Lekse J.W., Aitken J.A., *J. Solid State Chem.*, **180**(2007), 3262.
12. Larson P., Lambrecht R.L., *Phys. Rev. B.*, **78**(2008), 195207.
13. Janicek P., Drasar C., Lostak P., Vejpravova J., *Physica B*, **403**(2008), 3553.
14. Lostak P., Drasar C., Klichova I., Cernohorsky T., *Phys. Status Solidi B*, **200**(1997), 289.
15. Alemi A., Klein A., Meyer G., Dolatyari M., Babalou A., Z. *Anorg. Allg. Chem*., **637**(2011), 87.
16. Alemi A., Hanifehpour Y., Joo S.W., Min B., *Physicochem. Eng. Aspects*, **390**(2011), 142.
17. Alemi A., Hanifehpour Y., Joo S.W., Khandar A., Morsali A., Min B., *Physica B*, **406** (2011), 2801.
18. Makhov V.N., Batygov S.K., Dmitruk L.N., Kirm M., Vielhauer S., *Phys Solid State*, **50**(2008), 1625.
19. Zych E., Hreniak D., Strek W., *J. Phys. Chem. B*, **106**(2002), 3805.
20. Loh E., *Phys. Rev.*, **175**(1968), 533-536.
21. Strohheofer C., Polman A., *Opt. Mater*., **21**(2003), 705.
22. Hoven G.N., Elsken J.A., Polman A., Dam C., Uffelen K., Smit M.K., *Appl. Opt*., **36** (1997), 3338.

Supplementary data

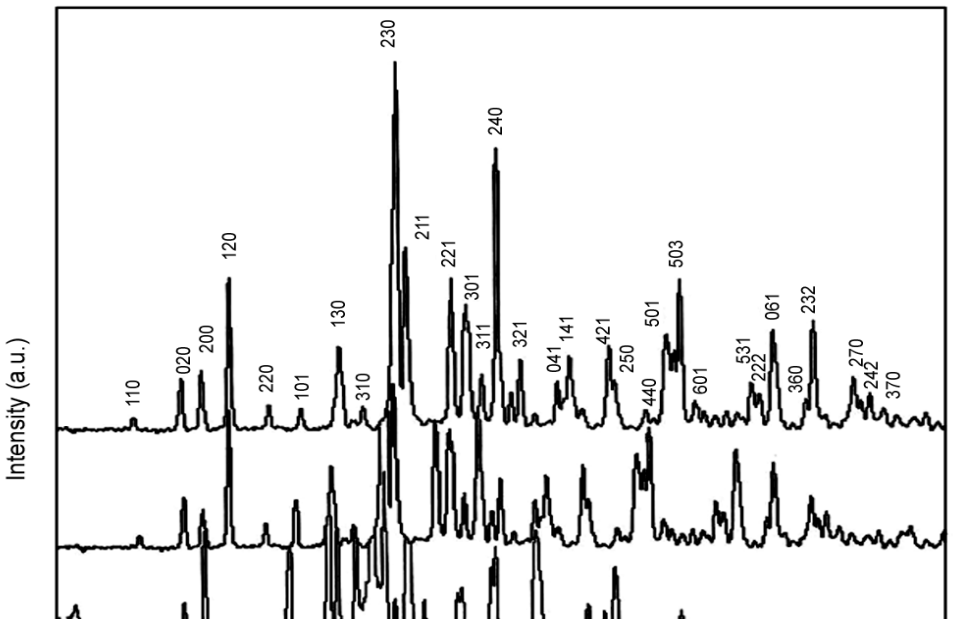

Figure 1: *Powder X-ray diffraction pattern of $Lu_xEr_xSb_{2-x}Se_3$ (x= 0.02).*

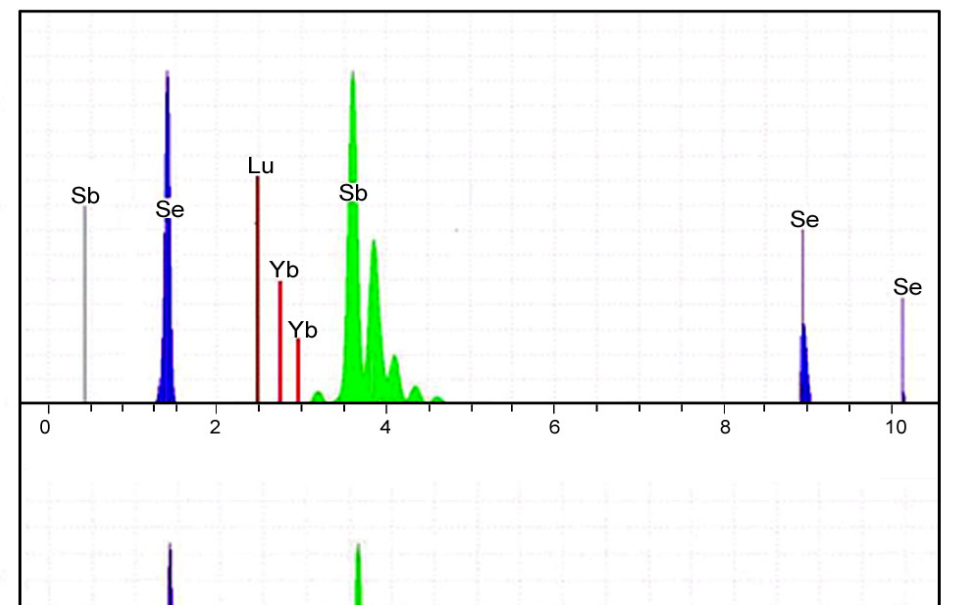

Figure 2: *Powder X-ray diffraction pattern of $Lu_xEr_xSb_{2-x}Se_3$ (x= 0.04).*

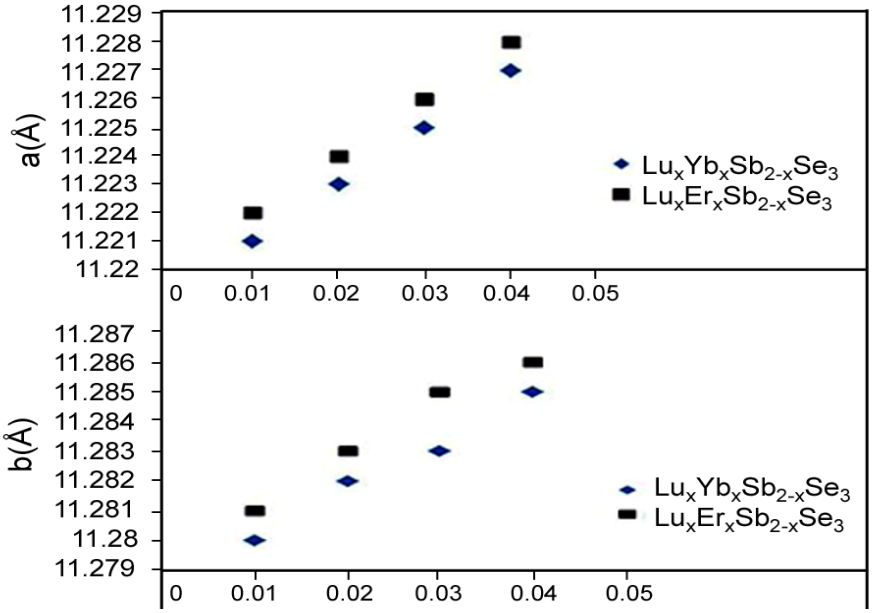

Figure 3: *Powder X-ray diffraction pattern of unknown $Lu_xEr_xSb_{2-x}Se_3$ phase.*

Figure 4: *TEM image of Sb_2Se_3 nanorods.*

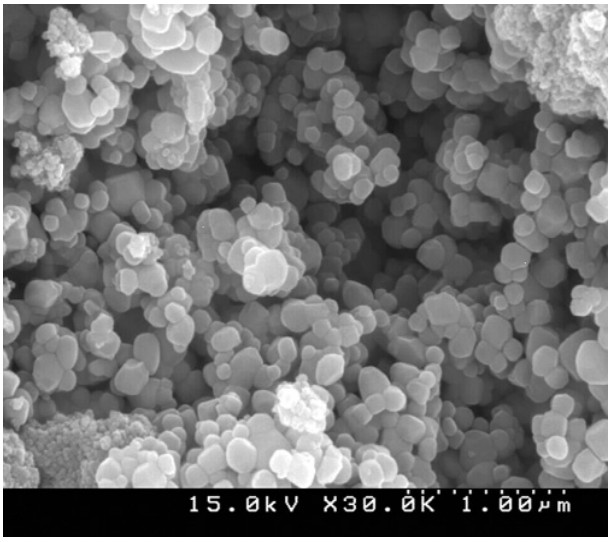

Figure 5: *HRTEM image of the Sb_2Se_3 nanorods.*

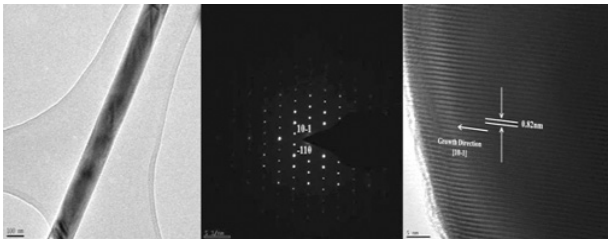

Figure 6: *SAED Pattern of the Sb_2Se_3 nanorods. The SAED zone axis is [10-1].*

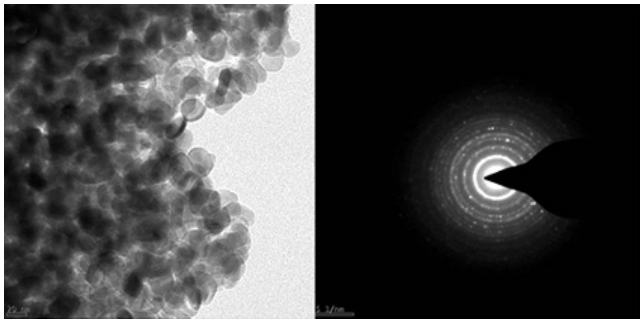

Figure 7: *Absorption spectra of $Lu_{0.02}Yb_{0.02}Sb_{1.96}Se_3$ nanorods at room temperature.*

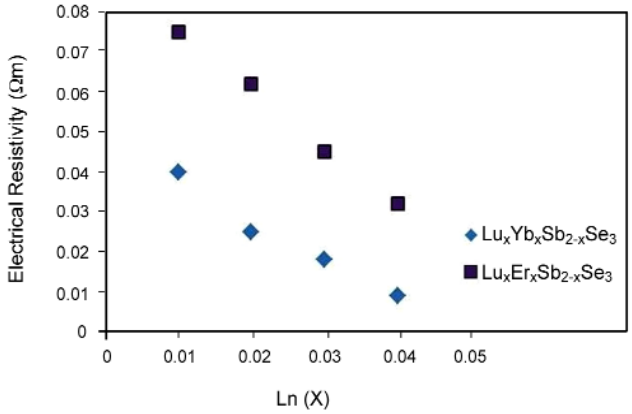

Figure 8: *Absorption spectra of $Lu_{0.01}Yb_{0.01}Sb_{1.98}Se_3$ nanorods at room temperature.*

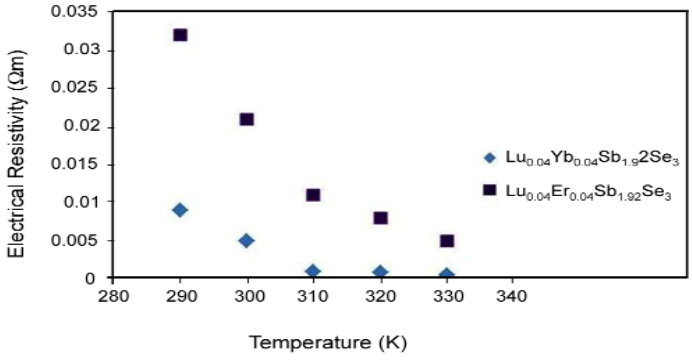

Figure 9: *Absorption spectra of $Lu_{0.02}Er_{0.02}Sb_{1.96}Se_3$ nanoparticles at room temperature.*